Géotechnique **00**, 1–6 [http://dx.doi.org/10.1680/geot.XX.XXXXX]

Understanding shear mechanisms in rooted soils using fibre-optic instrumented 3D-printed roots

G. SORRENTINO*‡[ORCID], J. A. REINERTSEN*, A. S. CHRISTIANSEN*[ORCID] and I. RASMUSSEN†

Vegetation can increase soil shear strength, yet the mechanisms governing root reinforcement remain difficult to quantify due to limited direct measurements. This communication presents a methodology that combines resin-based 3D-printed synthetic roots with distributed fibre-optic sensing to measure root deformation during direct shear tests in sand. Short and long bio-inspired root systems were tested in sand using resin mixtures with contrasting stiffness. Short roots produced a frictional response with similar peak strengths for stiff and flexible resins, consistent with their acting primarily as geometric asperities along the shear plane. In contrast, long roots generated higher shear resistance and an approximately linear increase in shear stress with displacement. Fibre-optic measurements revealed progressive mobilisation of tensile strain along the embedded length, indicating reinforcement through the formation of a soil–root composite tying the specimen halves together. The results demonstrate the potential of combining 3D printing and distributed sensing to investigate root–soil reinforcement mechanisms.

KEYWORDS: Rooted soil; Root reinforcement; fiber-optic sensing; 3D printing; Direct shear tests

INTRODUCTION

Vegetation is widely recognised as an important contributor to slope stability and erosion control (Lann et al., 2024; Meng et al., 2020). However, the mechanisms by which roots enhance soil shear strength remain difficult to quantify due to limited direct measurements (Giadrossich et al., 2017). Rooted soils can exhibit substantially higher shear resistance than unreinforced soils, yet limited experimental evidence is available (Bull et al., 2020) to determine whether this increase is primarily due to root pull-out, shearing of roots across the failure plane, or mobilisation of a soil–root composite that produces a cohesion-like response.

A key challenge in understanding root reinforcement is the complexity and variability of natural root systems. Roots exhibit heterogeneous geometries, branching patterns, and material properties that evolve with growth and environmental conditions (Bao et al., 2014), making it difficult to isolate controlling parameters or relate macroscopic shear behaviour to soil–root interactions. Synthetic roots with simplified or bio-inspired geometries have been used in direct shear and pull-out tests (de Sousa et al., 2024; Liang et al., 2018; Kim et al., 2024; Schlüter et al., 2025), but these approaches typically provide limited information on root deformation during shearing.

Recent advances in 3D printing and distributed fibre-optic sensing (Klar et al., 2019; Ma et al., 2023) offer a way to address this limitation. Resin-based stereolithography (SLA) allows root-like geometries to be reproduced with controlled stiffness, while optical frequency domain reflectometry (OFDR) provides continuous axial strain measurements along a fibre bonded to the root (Wang et al., 2025). Together, these techniques enable tracking of strain mobilisation along a synthetic root during shear, providing direct insight into the mechanisms of root reinforcement.

This communication presents a methodology combining resin-based 3D printing with distributed fibre-optic sensing to measure root deformation during direct shear tests. Salix roots (Otim et al., 2025b) were scanned to generate realistic synthetic branches, which were 3D printed, instrumented with a fibre-optic sensor, and sheared in sand using a rooted-soil shear apparatus. The objective is to demonstrate feasibility and to explore whether reinforcement is governed primarily by root pull-out or local root shearing. The root–soil stiffness ratio is not addressed and is left for future work.

MATERIALS AND METHODS

Rooted-soil shear apparatus (RSSA)

Shear tests were conducted using the Rooted Soil Shear Apparatus (RSSA) (Sorrentino et al., 2025). Specimens were prepared in PVC sections (100 mm inner diameter, 180 mm height) and tested under self-weight normal stress. Data acquisition and control were managed using an Arduino-based system.

Materials

Sand

The soil used was Dansand silica sand, poorly graded with a median grain size $d_{50} = 0.36\,\mathrm{mm}$, uniformity coefficient $U = 2.10$, and curvature $C_z = 0.95$ (Das, 2019; ASTM, 2017). Key properties are summarised in Table 1.

Resin and optical fiber

Synthetic roots were printed using commercial UV-curable resins for stereolithography. Two PrimaCreator formulations were employed: a relatively stiff, ABS-like resin (Value Tough UV Resin) and a more compliant resin (Value Flex UV Resin). Two materials with contrasting stiffness were produced while keeping the geometry unchanged: one printed entirely from the Tough resin (“100”) and one created by mixing equal parts of Tough and Flex (“50/50”).

Uniaxial tensile tests yielded tensile strengths of approximately 38 MPa for 100 and 21 MPa for 50/50 (Reinertsen, 2025; Otim et al., 2025a). A bare single-mode optical fiber (9/125 µm, ITU-T G.652D) was embedded along the 3D-printed roots for strain measurements.

Manuscript received...
*Technical University of Denmark, Department of Environmental and Resource Engineering, 2800 Kgs. Lyngby, Denmark.
†Technical University of Denmark, Department of Civil and Mechanical Engineering, 2800 Kgs. Lyngby, Denmark
‡E-mail: gs581@cantab.ac.uk

Table 1. Summary of physical and chemical properties of the tested sand (Sorrentino and Franza, 2025).

Property	Value	Unit	Description
Shape Descriptors			
Sphericity	0.82 (±0.037)	–	
Aspect Ratio	0.72 (±0.117)	–	
Convexity	0.96 (±0.016)	–	
Roundness	0.34 (±0.110)	–	
Particle Size Distribution			
D10	0.19	mm	Diameter at 10% passing
D30	0.27	mm	Diameter at 30% passing
D50	0.36	mm	Median diameter
D60	0.41	mm	Diameter at 60% passing
D90	0.54	mm	Diameter at 90% passing
Uniformity Coeff. (U)	2.10	–	D_{60}/D_{10}
Curvature Coeff. (C_z)	0.95	–	$D_{30}^2/(D_{10} \cdot D_{60})$
Chemical and Physical Properties			
SiO_2 content	99.08	%	Silicon dioxide content
Al_2O_3 content	0.457	%	Aluminum oxide content
Grain density	2.640	g cm^{-3}	
Bulk density	1460–1610	kg m^{-3}	Minimum to maximum bulk density

Table 2. Print settings for resin 3D printer (Reinertsen, 2025).

Parameter	Value	Unit
Layer height	0.05	mm
Bottom layer count	6	
Exposure time	6	s
Bottom exposure time	50	s
Light-off delay	0.5	s
Bottom lift distance	8	mm
Lifting distance	5	mm
Bottom lift speed	120	mm/min
Lifting speed	60	mm/min
Bottom retract speed	180	mm/min
Retract speed	90	mm/min

Synthetic root design and fabrication

The main steps in producing the synthetic roots are illustrated in Fig. 1. Salix root geometries were captured using an HDI 3D scanner (Polyga) with FlexScan 3D software (Fig. 1a). Roots were obtained from a previous experiment grown under controlled conditions by Otim et al. (2025b). Scanned meshes were cleaned and simplified in Blender 3D to generate printable models (Fig. 1b); the Blender files are available at https://github.com/jorei123/Root_Structure.

Optimised meshes were imported into Chitubox to define print orientation, support structures, and slicing parameters (Fig. 1c). Roots were printed using an Anycubic Photon Mono X SLA printer at 50 µm XY resolution and 10 µm nominal Z accuracy (Fig. 1d). SLA was chosen because preliminary PLA specimens printed by FDM exhibited defects and failures in thin regions and near mounting points, whereas SLA produced more homogeneous prints with easily removable supports.

SLA reproduced macroscopic geometric irregularities (curvature, local thickening, nodes, and small lateral branches), but microscale surface texture and friction were not captured. Capturing these features would require higher-resolution modelling and printing and was left for future work. Highly branched geometries required careful preparation of support structures and print orientation; an example is shown in Fig. 1e.

All specimens were printed using the same settings (Table 2) and post-processed by washing in isopropanol for 20 min using an Anycubic Wash & Cure Plus machine, followed by a further 20 min UV curing.

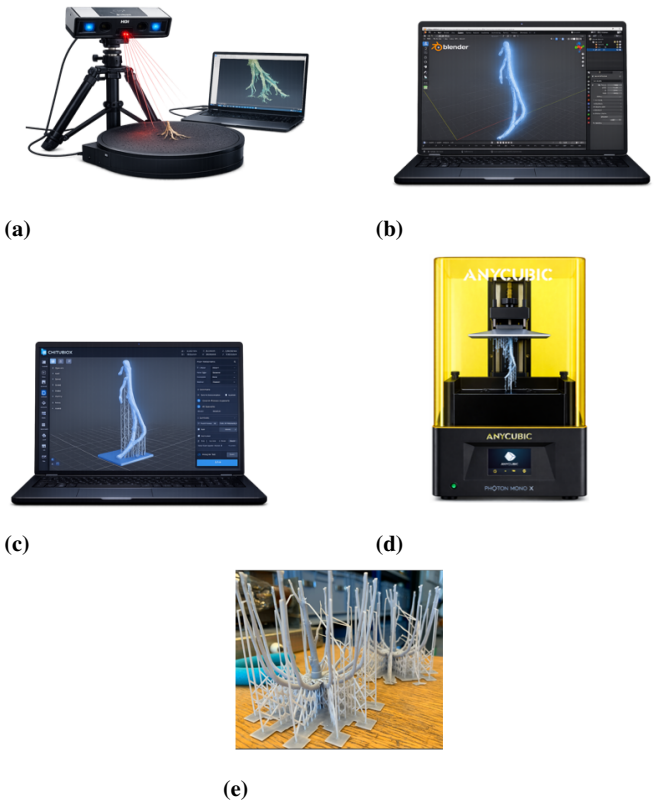

(a) (b) (c) (d) (e)

Fig. 1. Steps of the synthetic root design and fabrication.

Fiber-optic instrumentation

A bare single-mode optical fibre was bonded along one branch of each 3D-printed root. A baseline was recorded before each test, and axial strain was measured relative to this reference using a Luna OBR 4600 optical frequency domain reflectometer (OFDR) (Skar et al., 2019).

The fibre was attached using cyanoacrylate adhesive (instant glue, Green Stuff World) in short segments. It was first aligned along the branch and temporarily secured with small pieces of tape; glue was then applied over a few millimetres at a time until the full length was bonded (Fig. 2).

Prior to testing, the ends of the instrumented branch were located by applying a heated metal pin at selected positions

along the fibre, producing local peaks in the OFDR signal (Fig. 3).

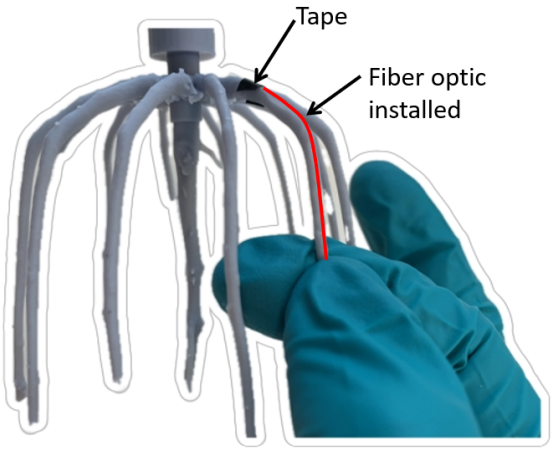

Fig. 2. Fiber-optic installation on 3D-printed root.

Specimen preparation and test procedure

Direct shear tests were performed on sand specimens containing the 3D-printed root geometry. The sand was prepared at a water content of approximately $w \approx 15\,\%$ and a relative density of $D_r \approx 30\,\%$ by pluviating the material into the PVC sections. Reference tests were also conducted on unreinforced sand specimens prepared using the same procedure.

Two embedment configurations were tested to examine whether the main contribution to shear strength arose from the portion of the root intersecting the shear plane or from the embedded portion within the soil: a "long" configuration, with the root extending well below the shear plane, and a "short" configuration, with minimal embedment. Both configurations were printed in the two resin mixtures described previously to investigate the effect of root stiffness. For instrumented tests, the fibre was bonded along the branch aligned with the shear direction, and all roots were positioned vertically in the sand.

Specimen assembly is illustrated in Fig. 4. The 3D-printed root system was positioned in the bottom half of the split PVC section, and its embedment depth was adjusted. Sand was then poured, the second half of the pipe assembled and secured with tape, and sand placement completed to the target height. Water was added to reach the desired content, and specimens were left at room temperature for approximately one hour. Finally, the PVC section was placed in the RSSA groove, the tape removed

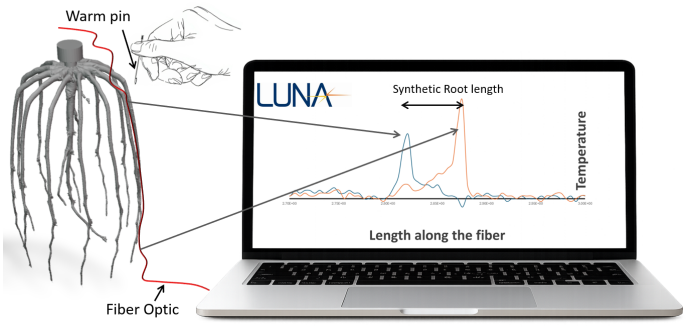

Fig. 3. Identification of the reference positions along the fiber-optic instrumented root.

to ensure a clear gap along the shear plane, and tests initiated with shear force, displacement, and fibre-optic strain recorded automatically at selected stages.

All shear tests were run to a horizontal displacement of $15\,\mathrm{mm}$. In the short-root configuration, larger displacements would have caused the root tip to contact the stationary half of the PVC section; for consistency, results for the long-root configuration are also reported up to $15\,\mathrm{mm}$.

After testing, specimens were dismantled and the synthetic roots inspected visually. Pronounced bending and branch distortion were observed (Fig. 5), confirming significant root deformation during shearing. Although not quantified, these observations suggest that post-test imaging could complement fibre-optic measurements in future studies.

RESULTS AND DISCUSSION

Fig. 6 shows the shear stress–displacement response for unreinforced sand and for sand reinforced with the synthetic root system. Tests are labelled by root configuration (Long or Short) and resin type (100 = stiff, 50/50 = flexible), with T# indicating the test number; reference tests on sand alone are denoted Sand_T#.

Roots increased shear strength relative to unreinforced sand. In the short-root configuration, both resins produced a typical frictional response: shear stress rose to a peak and then remained approximately constant, with no clear difference in peak strength between materials. This suggests that when the root was embedded only a few millimetres below the shear plane, it acted primarily as a geometric asperity, and its stiffness was not effectively mobilised. In contrast, the long-root configuration exhibited approximately linear hardening, consistent with trends reported for natural roots (Bull et al., 2020; Davoudi, 2011; Sorrentino et al., 2025), and dependent on resin type: the more flexible material mobilised higher shear strength over the displacement range.

The duplicate direct shear tests (T1 and T2) display closely matching τ–δH curves, indicating good repeatability and low inter-test variability. The coefficient of variation was 2.02% for the long-root configuration, 4.42% for the short-root flexible configuration, and 2.29% for the short-root rigid configuration.

Fig. 7 presents axial strain along the fibre-optic instrumented root at different displacement stages. The largest strains occurred just above the shear plane, but measurable strain was observed along the full root length, including the embedded section. For long roots (Fig. 7a, Fig. 7b), strain along the embedded portion increased progressively with displacement, indicating that the root was mobilised in tension. As the upper half of the specimen was displaced, the confined root was pulled against the surrounding sand, mobilising resistance along the root–soil interface and in the surrounding soil, effectively tying the specimen halves together. This mechanism explains the approximately linear increase in shear stress and the cohesion-like behaviour of the soil–root composite. Strain measurements for the long-root flexible resin were noisier, reflecting the preliminary stage of the fibre-optic acquisition, but the qualitative trend remained.

For the short-root configuration (Fig. 7c, Fig. 7d), strain increased with displacement and peaked just above the shear plane. Beyond $5\,\mathrm{mm}$ of horizontal displacement, strain profiles remained nearly constant, as the embedded portion was too short to develop the progressive pulling observed in long roots. The flexible root exhibited larger deformations than the stiffer one due to greater material compliance under the same load.

Together, the shear-test results and fibre-optic measurements indicate that roots intersecting only the shear plane provide a modest, predominantly frictional contribution to shear strength,

Fig. 4. Main stages in specimen preparation and installation in the RSSA: (a) root system positioned in the lower half of the split PVC pipe; (b) root embedment depth adjusted to the target level; (c) sand poured into the first half of the cylinder; (d) second half of the PVC pipe assembled and secured with tape; (e) sand placement completed to the target height; (f) water added and specimen left at room temperature for 1 h; (g) PVC section placed in the RSSA groove; (h) tape removed and a gap is ensured along the shear plane; (i) direct shear test started with RSSA measurements and fiber-optic readings.

Fig. 5. Post-test configuration of the 3D-printed synthetic root system, showing bending and distortion of the branches after shearing.

whereas deeper, embedded roots contribute substantially through a cohesion-like effect associated with holding the two specimen halves together during shearing.

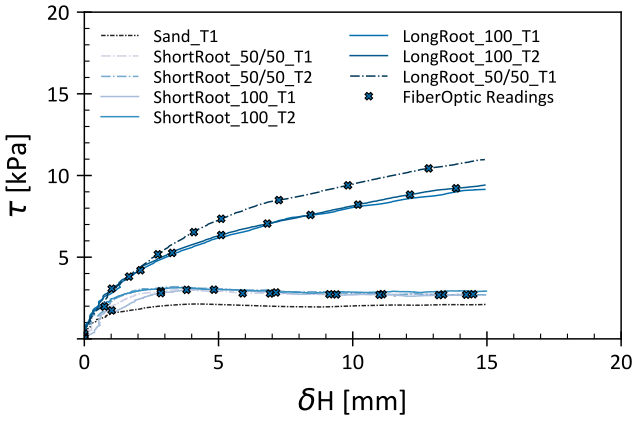

Fig. 6. Comparison of shear behaviour for sand and sand reinforced with 3D-printed roots of varying material and length.

CONCLUSIONS

This study demonstrates that combining resin-based 3D-printed roots with distributed fibre-optic sensing provides continuous strain measurements along roots and allows identification of the dominant reinforcement mechanisms in rooted soils.

Roots intersecting only the shear plane produced a modest, predominantly frictional increase in shear strength. In contrast, longer roots embedded below the shear plane generated substantially higher shear resistance and an approximately linear hardening response. Fibre-optic measurements revealed progressive mobilisation of tensile strain along the embedded length, indicating tension mobilisation rather than local root shearing at the imposed plane. This behaviour is consistent with the development of a soil–root composite that effectively ties the specimen halves together, producing a cohesion-like contribution to shear strength.

Although the present dataset is limited, these preliminary results highlight the potential of combining 3D printing and distributed sensing as a methodology for probing root reinforcement mechanisms, providing a foundation for future studies and more detailed parametric investigations.

ACKNOWLEDGEMENTS

This work partially funded by the Carlsberg Foundation under the Semper Ardens: Accelerate Consolidator Excellence Grant, through SOil Is Alive (SoIA) project.

AUTHOR CONTRIBUTIONS

Gianmario Sorrentino: Conceptualisation, Data curation, Formal analysis, Investigation, Methodology, Supervision, Validation, Visualisation, Writing - original draft. **Jørgen Aske Reinertsen:** Data curation, Formal analysis, Investigation. **Asmus Skar Christiansen:** Methodology, Writing - review & editing. **Ian Rasmussen:** Methodology.

REFERENCES

ASTM. Astm d2487-17e1: Standard practice for classification of soils for engineering purposes (unified soil classification system). Astm, 2017.

Yun Bao, Pooja Aggarwal, Neil E Robbins, Craig J Sturrock, Mark C Thompson, Han Qi Tan, Cliff Tham, Lina Duan, Pedro L Rodriguez, Teva Vernoux, et al. Plant roots use a patterning mechanism to position lateral root branches toward available water. *Proceedings of the National Academy of Sciences*, 111(25):9319–9324, 2014.

DJ Bull, JA Smethurst, Ian Sinclair, Fabrice Pierron, Tiina Roose, William Powrie, and Anthony G Bengough. Mechanisms of root reinforcement in soils: an experimental methodology using four-dimensional x-ray computed tomography and digital volume correlation. *Proceedings of the Royal Society A*, 476(2237): 20190838, 2020.

Braja M Das. *Advanced soil mechanics*. CRC press, 2019.

Mohammad Hadi Davoudi. Influence of willow root density on shear resistance parameters in fine grain soils using in situ direct shear tests. *Research Journal of Environmental Sciences*, 5(2):157, 2011.

Raul Batista Araujo de Sousa, Anthony Kwan Leung, Jonathan Adam Knappett, and Xingyu Zhang. Strength and stiffness anisotropy of 3d-printed coarse root analogues for small-scale physical modelling. *Géotechnique Letters*, 14(4):139–144, 2024.

F Giadrossich, M Schwarz, D Cohen, A Cislaghi, C Vergani, T Hubble, C Phillips, and Alexia Stokes. Methods to measure the mechanical behaviour of tree roots: A review. *Ecological engineering*, 109: 256–271, 2017.

Yoon-Ah Kim, Matthew Burrall, Min-Kyung Jeon, Jason T DeJong, Alejandro Martinez, and Tae-Hyuk Kwon. Pullout behavior of tree root-inspired anchors: development of root architecture models and centrifuge tests. *Acta Geotechnica*, 19(3):1211–1229, 2024.

Assaf Klar, Michael Roed, Irene Rocchi, and Ieva Paegle. Evaluation of horizontal stresses in soil during direct simple shear by high-resolution distributed fiber optic sensing. *Sensors*, 19(17):3684, 2019.

Tongsan Lann, Han Bao, Hengxing Lan, Han Zheng, Changgen Yan, and Jianbing Peng. Hydro-mechanical effects of vegetation on slope stability: A review. *Science of the Total Environment*, 926: 171691, 2024.

Teng Liang, JA Knappett, GJ Meijer, D Muir Wood, AG Bengough, KW Loades, and PD Hallett. Scaling of plant roots for geotechnical centrifuge tests using juvenile live roots or 3d printed analogues. In *Physical Modelling in Geotechnics, Volume 1*, pages 401–406. CRC Press, 2018.

Jiaxiao Ma, Huafu Pei, Honghu Zhu, Bin Shi, and Jianhua Yin. A review of previous studies on the applications of fiber optic sensing

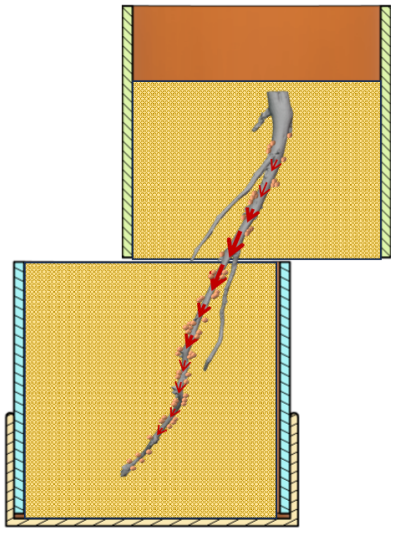

Fig. 8. Schematic interpretation of the long-root configuration during shearing. The red arrow indicates tensile mobilisation of the root, while the blue arrows represent reaction forces in the surrounding soil, illustrating the development of a soil–root composite across the shear plane.

technologies in geotechnical monitoring. *Rock Mechanics Bulletin*, 2(1):100021, 2023.

Suyun Meng, Guoqing Zhao, and Yuyou Yang. Impact of plant root morphology on rooted-soil shear resistance using triaxial testing. *Advances in Civil Engineering*, 2020(1):8825828, 2020.

G. I. Otim, Gianmario Sorrentino, J. A. Reinertsen, A. Zhelezova, S. Trapp, and I. Rocchi. Systematic evaluation of tensile strength for natural and synthetic plant roots for soil reinforcement applications. In *Proceedings of RootS25: 3rd International Workshop on Soil-Vegetation-Atmosphere Interaction*, 2025a. doi: 10.53243/RootS2025-46.

Gerald Innocent Otim, Alena Zhelezova, Gianmario Sorrentino, Stefan Trapp, and Irene Rocchi. Hydraulic properties of rooted soils from salix sp. pot experiments. In *E3S Web of Conferences*, volume 642, page 06009. EDP Sciences, 2025b.

Jørgen Aske Reinertsen. Evaluating tensile stregth and deformation of 3d printed synthetic plant roots for geotechnical applications. Master's thesis, Danmarks Tekniske Universitet, 2025.

V. Schlüter, S. Wolski, and O. Stelzer. Root characteristics of willows on waterway banks. In D. Boldrin, M. Cecconi, F. Cotecchia, A. Leung, G. Pedone, P. Perrini, E. Romero, V. Tagarelli, and L. Zdravković, editors, *Proceedings of RootS25: 3rd International Workshop on Soil-Vegetation-Atmosphere Interaction*, 2025. doi: 10.53243/RootS2025-5.

Asmus Skar, Assaf Klar, and Eyal Levenberg. Load-independent characterization of plate foundation support using high-resolution distributed fiber-optic sensing. *Sensors*, 19(16):3518, 2019.

Gianmario Sorrentino and Andrea Franza. Experimental study of sugar-induced sand cementation in dry conditions. *Geomechanics for Energy and the Environment*, page 100765, 2025.

Gianmario Sorrentino, Gerald Innocent Otim, Alena Zhelezova, and Irene Rocchi. Rooted soil shear apparatus: A low-cost, direct shear apparatus for measuring the influence of plant roots on soil shear strength. *HardwareX*, page e00726, 2025.

Youqiang Wang, Dahan Guo, Jianbo Xu, Zhengyu Liu, Longfei Wang, and Chunhui Chen. Quantitatively analyzed root system architecture influence on root-soil mechanical interactions using 3d printing models. *Plant and Soil*, pages 1–18, 2025.

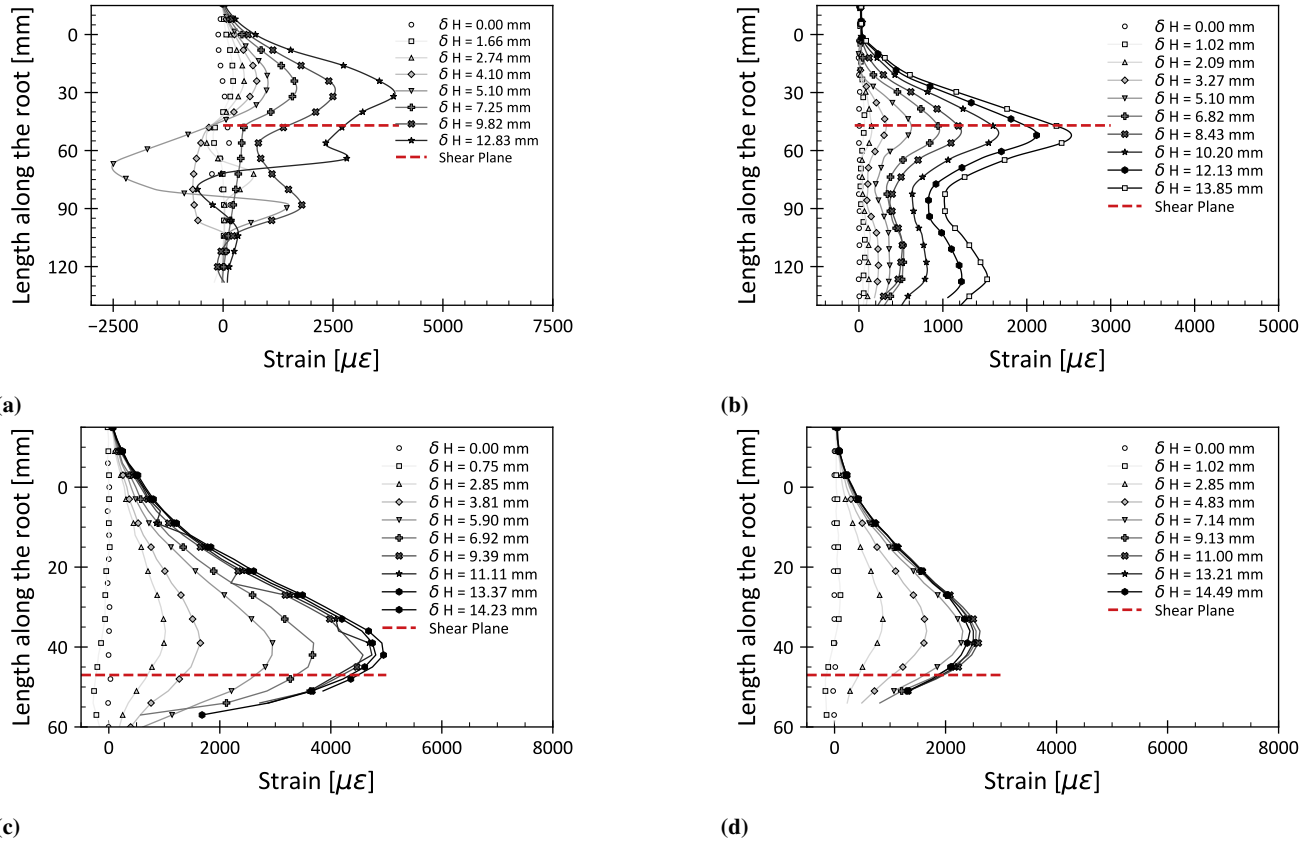

Fig. 7. Distributed axial strain along the fibre-optic instrumented root at different horizontal displacements, ΔH, during the direct shear test: (a) LongRoot-50-T1; (b) LongRoot-100-T1; (c) ShortRoot-50-T1; (d) ShortRoot-100-T1.